Fall 2020

Seasonal Differences in the Optical Properties of Chromophoric Dissolved Organic Matter at Hoag's Pond, WA

Kimberly Wallace
Western Washington University

Seasonal Differences in the Optical Properties of Chromophoric Dissolved Organic Matter at Hoag's Pond, WA

Kimberly Wallace, Catherine Clark: Department of Chemistry, Western Washington University, Bellingham, WA

Abstract:

Dissolved organic matter (DOM) plays an important role in carbon cycling in lakes and ponds. DOM sources may vary with elevation due to vegetation differences. To examine this, optical properties of chromophoric dissolved organic matter (CDOM) were investigated between a season with heavy rainfall (wet season) and a season without much rainfall (dry season) in Hoag's Pond, Washington, USA. This is the first study of CDOM optical properties on Hoag's pond. Data shows that there is an increase of CDOM in Hoag's Pond during wet season as compared to dry. Three-dimensional fluorescence excitation-emission matrices (EEM's) showed that Hoag's Pond contains allochthonous terrestrial humic-like peaks A and C. Fluorescence intensities were higher for wet season samples than dry season samples, indicating an increase of CDOM between seasons. Two fluorescence indices obtained from EEMs showed no statistically significant difference between dry and wet season; FI ranged from 1.28-1.3, indicating terrestrial material, and the BIX average was 0.66, indicating limited autochthonous contributions. The HIX index however was statistically significantly lower for dry season (3.46 as compared to 4.64), suggesting a higher proportion of autochthonous non-humic material during dry season. Water probe data indicates that conductivity (maximum 793µS ± 1% FS versus 1382µS ± 1% FS), total dissolved solids (maximum at 435ppm ± 1% FS versus 982ppm ± 1% FS), and salinity (maximum at 0.31ppt ± 1% FS versus 0.69 ppt ± 1% FS) values are statistically significantly higher for wet season, indicating a higher proportion of electrolytic, conductive material during wet season. The pH changes between seasons were not statistically significantly different, as the pH ranged from 6.34-7.30 ± 0.02 pH unit. These findings are consistent with increased inputs of allochthonous terrestrial material and decreased sources of autochthonous material between the transition from dry to wet season.

1. Introduction:

Lakes and ponds play an important role in global carbon cycling, with over 300 million lakes estimated to occur globally (Tranvik et al., 2009). Carbon cycles through lake waters through both photolysis and biological processing like respiration (Urban et al., 2005), in conjunction with physical processes like flocculation and settling. Fresh water bodies act as both a sink for

carbon through the storage of carbon-containing species in sediments, and a source of carbon to the atmosphere through the mineralization of dissolved organic matter (DOM) produced from bio-organisms in situ and in the surrounding catchment. Lakes and other freshwater bodies thus act as a mechanism to receive and transform carbon-containing terrestrial material prior to transferring it to rivers and coastal waters.

DOM plays an important role in biogeochemical cycling in natural water systems and supports aquatic food webs (Hessen and Tranvik, 1998). Upon exposure to solar radiation, DOM produces a range of reactive transient products in water that impact aquatic chemical cycles (Vione et al., 2014). It consists of very large water-soluble organic molecules with complex structures that include aromatic and aliphatic moieties (Nebbioso and Piccolo, 2013). DOM undergoes photochemical, physical, and microbial processing that affect its molecular characteristics and bioavailability (Moran and Zepp, 1997; Obernosterer and Benner, 2004). DOM is produced in natural water systems from both terrestrial plant and aquatic microbial sources (McKnight and Aiken, 1998). In a study of a lake ecosystem, autochthonous and allochthonous sources could be differentiated in the lake water based on molecular characterization (Bittar et al., 2015).

Chromophoric dissolved organic matter (CDOM) is the light-absorbing component of DOM (Green and Blough, 1994). CDOM attenuates ultraviolet radiation in lakes and ponds, providing some protection to organisms (Laurion et al., 2000). CDOM in lakes and ponds is primarily of allochthonous terrigenous origin, but some characteristics point towards the presence of autochthonous DOM from microorganisms or macrophytes and the alteration of terrigenous material by biological and photochemical processing (Urban et al., 2005). For example, decomposition and degradation of phytoplankton was shown to be an important source of CDOM in a study on a eutrophic shallow lake (Zhang et al., 2009). Lakes at high elevation above the tree line would be expected to have low allochthonous inputs from terrestrial material as they are surrounded by bare rock; lakes at low elevation below the tree line have high allochthonous inputs as they are surrounded by meadows and trees (Laurion et al., 2000; De Laurentiis et al., 2012).

CDOM’s optical properties have been used to assess levels, differentiate between allochthonous and autochthonous sources, and track biological and photochemical transformations of DOM. Common optical methods used to characterize CDOM include absorbance spectra, fluorescence

intensity measurements, calculations of spectral slopes and indices based on fluorescence and absorbance data, and three-dimensional excitation and emission matrix (EEMs) fluorescence spectra. Optical properties vary with the structure of DOM (Boyle et al., 2009). Absorption measurements allow for the estimation of CDOM levels in lakes by remote sensing techniques (Kutser et al., 2005). Spectral slopes and absorbance and fluorescence-based indices have been used to track the sources and transformation of CDOM (Green and Blough, 1994; Boyd and Osburn, 2004; Del Vecchio and Blough, 2004; Helms et al., 2008; Clark et al., 2014). DOM fluorescence (fluorescent DOM or FDOM) has been used to determine the sources and transport of DOM in coastal waters (Stedmon et al. 2003), and has been shown to vary with surrounding land cover for lakes (Zhao et al., 2017; Song et al., 2019). Optical properties of FDOM vary from groundwater to river to lake water (Mostofa et al., 2007). Coble (1996) first identified three humic-like and two protein-like peaks in EEM fluorescent spectra; these are attributed to allochthonous terrestrial material and autochthonous material produced in situ. Parallel factor analysis (PARAFAC) of EEM spectra has been used to identify additional or different components (see for example Qui et al., 2005). Fluorescent properties from EEM spectra are different for different source materials, for example showing differences between river and lake waters (Hayakawa et al., 2004). EEMs have been used extensively to characterize CDOM (see for example Clark et al, 2008), and to distinguish between allochthonous and autochthonous sources in natural waters (Stedmon and Markager, 2005).

In this study, we measured the optical properties of Hoag's Pond between wet and dry seasons in Washington State, USA. Additionally, we collected water probe data on the chemical properties of the water in Hoag's Pond. We hypothesized that there would be an increase of allochthonous terrestrial material in Wet season when compared to dry season. This is the first study of CDOM optical properties on this pond.

2. Materials and Methods

2.1 Sampling Figures: Figure 1 provides a map of the study site in northwestern Washington state in the USA. Samples were taken weekly from July 14th, 2020 to November 24th, 2020, with dry season denoted as July 14th 2020 to September 8th, 2020 and wet season denoted as September 24th, 2020 to November 24th, 2020. Seasonal boundaries were defined by recurring rain events, as measured by the Bellingham International Airport Weather Station, with the

transition to wet season beginning with a five-day streak of at least 0.75cm of continued rainfall (Figure 2).

Samples of surface water were collected in amber glass bottles from the shoreline at a single access point. Samples were vacuum filtered through Durapore 0.22-micron PVDF membrane filter to remove debris and microorganisms before measuring optical properties. All samples were stored in glass bottles and kept in the dark under refrigeration prior to analysis. Samples were analyzed immediately after vacuum filtration.

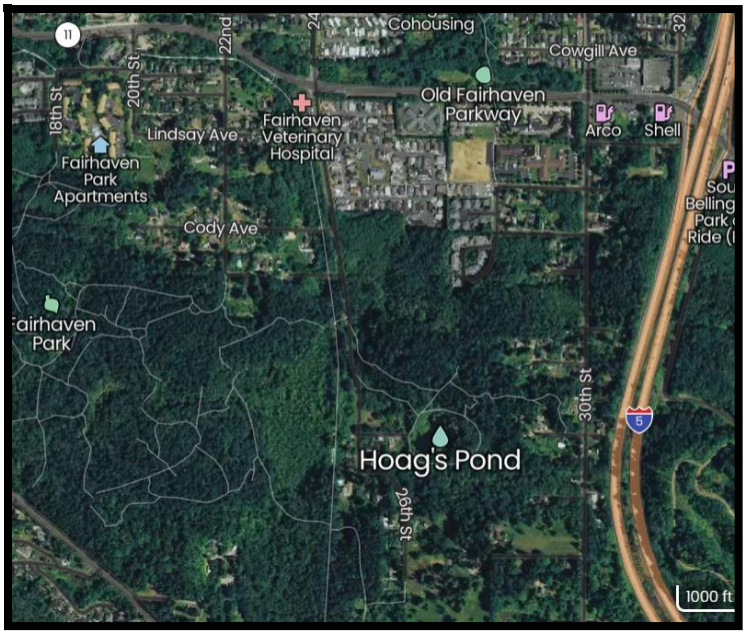

Figure 1: Map of Hoag's Pond obtained from MapCarta. The Study Site is located at 48.7079° N, 122.4833° W.

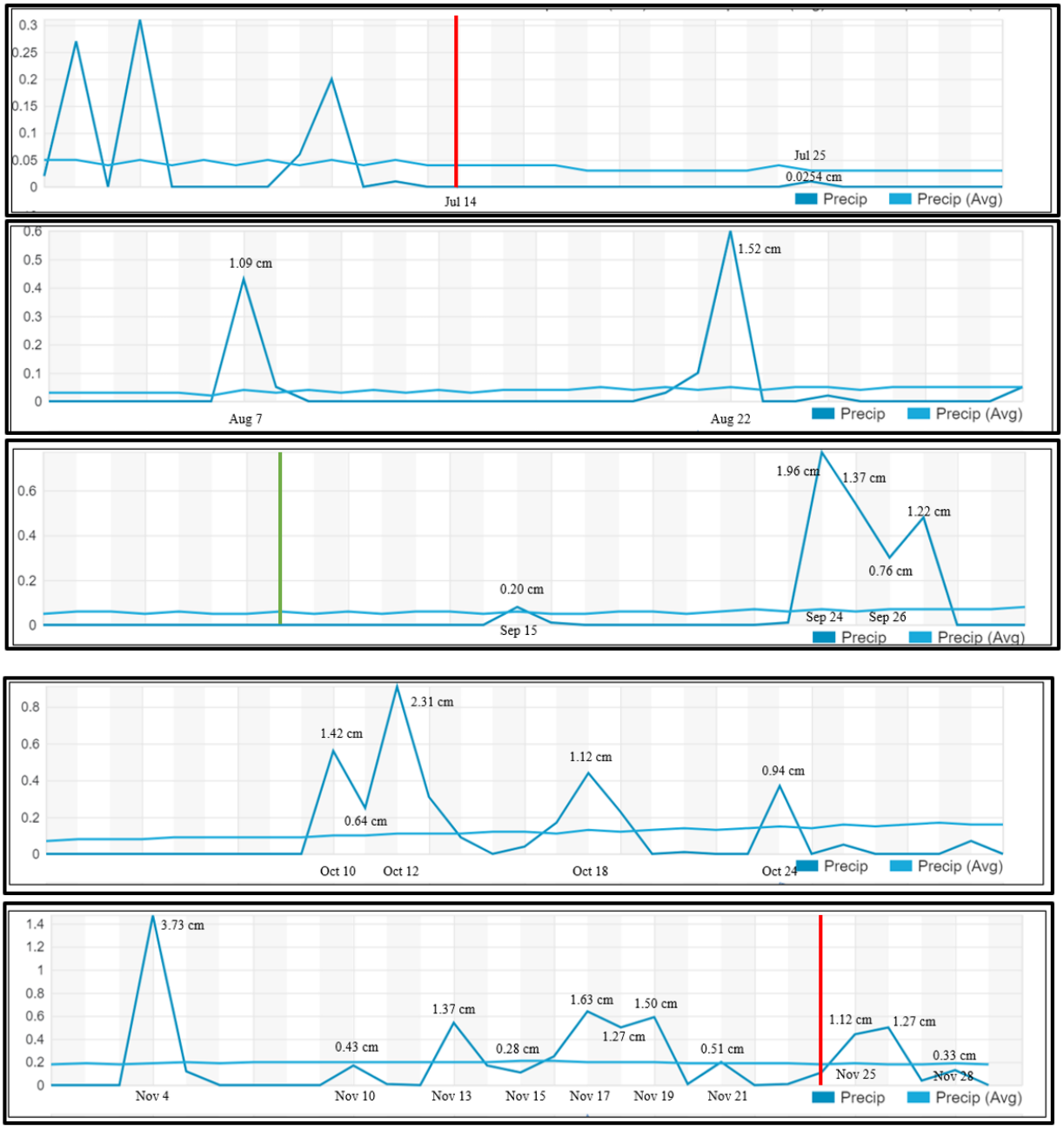

Figure 2: Precipitation values in Bellingham, Washington, USA from July 2020 through November 2020 as charted by the Bellingham International Airport Weather Station. The start and end dates for the study were denoted with a red line, with the transition between dry and wet season denoted with a green line. Rainfall data is plotted as inches on the y axis with each day on the x axis, however major rain events have been labeled by date with the precipitation amount in centimeters.

2.2 Fluorescence: EEM's were acquired using a HORIBA Aqualog fluorometer. Samples were analyzed in uncapped quartz fluorescence cells with a path length of 1 cm. The instrument has a wavelength accuracy of ± 1 nm and an effective analysis range from 230-800 nm (HORIBA). The light source is a 150W ozone-free xenon arc lamp. The Aqualog uses a TE-cooled CCD fluorescence emission detector which allows for ultrafast and simultaneous measurement of both absorbance and fluorescence. Instrument software corrects for inner filter effects (Ohno, 2002) and 1st order Rayleigh scattering. EEM's were collected with a resolution of <2 nm with stray light < 0.03% over an excitation range of 250-450 nm and an emission range of 260-800 nm. Nanopure water was used as a blank for all measurements. Each sample was collected with an integration time of 0.1 seconds. All samples were measured with the high gain setting (2.25 e^- /cts) on the CCD detector. A nanopure water blank was acquired once during the study and the integrated Raman peak area for water was used to obtain a conversion factor for the microvolt output of the instrument into the Raman units used in the results (RU; Lawaetz and Stedmon 2009).

The fluorescence index (FI), humification index (HIX), and the index of recent autochthonous contribution (BIX) were calculated using values from the processed EEM's. The fluorescence index, the ratio of emission at 450 nm to emission at 500 nm for excitation at 370 nm, can differentiate between microbial and terrestrial sources and is a useful indicator of the aromaticity of the sample. In general, the lower the fluorescence index, the more aromatic the material. The FI value is about 1.9 for aquatic and microbial sources and 1.2-1.3 for terrestrial and soil sources (McKnight et al., 2001; Huguet et al., 2009). HIX is the ratio of the peak emission intensities from 435-480 nm and from 300-345 nm at an excitation wavelength of 254 nm. It is a useful indicator for the degree of humification within a sample and gives information about the degree of CDOM processing (Zsolnay et al., 1999; Chen et al., 2011). BIX is calculated at an excitation wavelength of 310 nm from the ratio of the emission intensities at 380 nm and 430 nm. This index corresponds with CDOM production and therefore gives information about recent biological activity in a marine system (Huguet et al., 2009).

2.3 *Absorbance:* The Aqualog spectrometer measures absorbance at the same time as fluorescence and uses the same wavelength range. Napierian absorption coefficients were calculated from the absorbance data using equation 1 below (Hu et al., 2002):

$$\alpha = \frac{2.303}{L} \cdot A(\lambda) \qquad (1)$$

where A(λ) is the measured absorbance at the specified wavelength, α is the Napierian absorption coefficient, and L is the path length of the quartz cell in meters. Spectral slopes (S) were calculated by fitting data for S1 (300-400 nm), S2 (275-295 nm), and S3 (350-450 nm) to equation 3 below. The slope ratio (S_R) is calculated as the ratio of S2 to S3 (Helms et al. 2008):

$$-S = \frac{\ln\left(\frac{A}{A_0}\right)}{(\lambda - \lambda_0)} \qquad (3)$$

(A) is the absorbance at wavelength λ and A_o is the absorbance at reference wavelength λ_o.

2.4 *Water Probe Data:* The Pocket Pro+ Multi 2 Tester measures the pH, conductivity, total dissolved solids (TDS), and salinity of a water sample. In terms of accuracy, the pH value is reported within ± 0.02 pH unit and the conductivity, TDS, and salinity values within ±1% FS. The probe was inserted into the sample and stabilized values were recorded for each sample date.

3. Results:

3.1 *Water probe data:* For dry season, from July 14th to September 8th, 2020, pH values ranged from 6.34-6.97 (average 6.76 ± 0.21 (1σ)) whereas in wet season, from September 24th to November 24th, 2020, pH values ranged from 6.61 to 7.30 (average 6.92 ± 0.19 (1σ)), indicating a statistically insignificant (P-value 0.059) difference in pH value from dry to wet season. For dry season, conductivity values varied from 156.6μS to 793.0μS (average 318.3 ± 243.3μS (1σ)) while in wet season, conductivity values varied from 332μS to 1382μS (average 586.3 ± 318.4μS (1σ)), indicating a statistically significant (P-value 0.036) increase in conductivity from dry to wet season. Similarly, total dissolved solids (TDS) values in dry season ranged from 111ppm to 563ppm (average 226 ± 172.7 ppm (1σ)), while in wet season, TDS values ranged from 234ppm to 982ppm (average 416.7 ± 226.3 ppm (1σ)), revealing a statistically significant (P-value 0.036) increase in TDS from dry to wet season. Furthermore, salinity values in dry season ranged from 0.08 ppt to 0.4 ppt (average 0.16 ± 0.12 ppt (1σ)), while in wet season, TDS values ranged from 0.16 ppt to 0.69 ppt (average 0.29 ± 0.16 ppt (1σ)), revealing a statistically significant (P-value 0.038) increase in salinity from dry to wet season.

3.2 *Fluorescence data:*

Different peaks in excitation-emission spectra have been identified over time and are correlated with the type and origin of fluorophore (Coble, 2007). Signals associated with terrestrial and marine humic-like material and autochthonous protein-like material have been identified in EEMs and are referred to in the literature by their alphabetical designation. (A, C, M, T and B; Coble. 2007). Figure 4 shows a typical example of an EEM spectrum for a lake. The wavelengths used to assign peaks in the EEMs are given in Coble (1996). Increasing fluorescence intensities indicates higher levels of FDOM in the water.

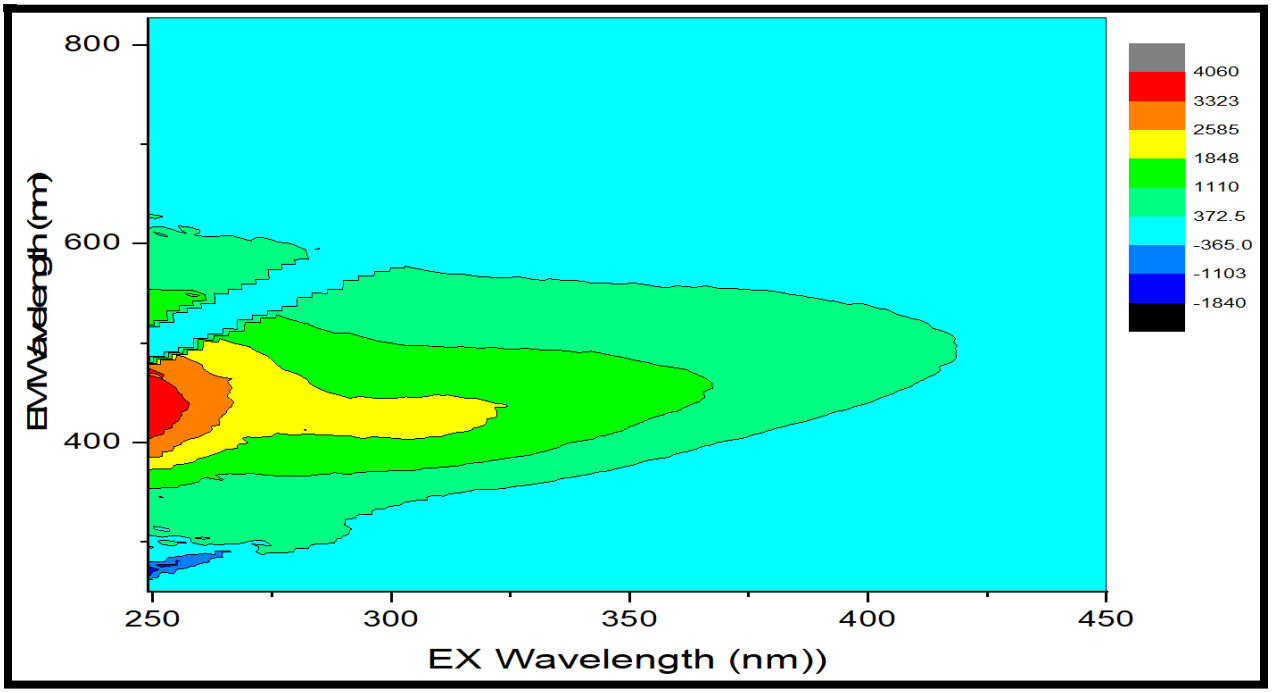

Figure 4. An EEM for Hoag's Pond in wet season, typical of the spectra measured in the entirety of the study. Peaks A and C are labelled. Peaks A and C are characteristic of allochthonous terrestrial humic-like material. Intensity values are measured in counts per second.

Peak A (Ex 260: Em 450) which corresponds to the humic portion of the CDOM pool was found in all samples of the study. This peak is typically associated with terrestrially sourced allocthonous CDOM (Coble, 2007). Average peak A intensities were 3119.8 ± 440.5 counts per second for the dry season and higher at 7802.0 ± 5626.9 counts per second for the wet season (Table 1). This data continues the trend of dry season samples having lower fluorescence intensity, suggesting a lower concentration of fluorescent optically active CDOM as compared to wet season.

Humic Peak C (Ex 340: Em 440) which has been identified in the past as representing a terrestrial source of CDOM was found in all samples. This makes sense as the two humic peaks (A and C) are generally found with one another (Kowalczuk et al., 2005). Average peak C intensities were lower than humic peak A, with the dry and wet season groupings having corresponding average values of 1378.8 ± 440.5 counts per second and 3390.9 ± 2585.0 counts per second (Table 1). The two means are statistically different at a 95% confidence level (student t-test).

Peak T is typically associated with the amino acid tryptophan and is referred to in the literature as a protein-like peak (Osburn et. al., 2011). This is considered an indicator of autochthonous production from microbial sources (see for example Hayakawa et al., 2016). Peak T was observed in two of the sixteen samples, July 20th, 2020 and August 11th, 2020, both dates in dry season. The protein-like peak had lower intensities on average compared to peaks A and C. The two peaks measured at 2092.0 and 980.1 counts per second, respectively (Table 1).

Peak ratios were calculated (Table 1). This type of inquiry provides information on the primary CDOM source in a sample (Kieber et al., 2005). The A to C ratio (A/C) had an average of 2.31 ± 0.25 for dry season. Wet season samples showed a similar average of 2.33 ± 0.17.

Other fluorescence parameters such as the fluorescence index, humification index, and biological index values were calculated (Table 1). FI values averaged 1.30 ± 0.044 for dry season and 1.28 ± 0.034 for wet season. BIX values averaged 0.71 ± 0.034 for dry season and 0.61 ± 0.40 for wet season. Some variation was observed for HIX between the two seasons, which had an average of 3.46 ± 1.45 for dry season and 4.64 ± 0.67 for wet season. Statistical analysis showed the HIX data for high and low altitude classifications to be significantly different from each other (t-test); however, the difference for FI and BIX was not significant at a 95% confidence level.

3.3 *Absorbance data:* Optical characterization results can be found in (Table 2). Results are separated by absorbance and fluorescence data for both seasons. Absorption coefficients are an indicator of the relative amounts of CDOM in the water. Dry season had α_{350} values ranging from 13.9 to 18.0 m^{-1} (average 16.03 m^{-1} ± 1.36 m^{-1}). Wet season had higher α_{350} values ranging from 25.17 to 67.24 m^{-1} (average 45.98 m^{-1} ± 15.47 m^{-1}). Both data sets had p-values <0.05, indicating a statistically significant correlation. The wet and dry season data sets were statistically significantly different (student t-test).

Spectral slopes indicate the rate at which CDOM absorption declines with increasing wavelength over various ranges. These changes have been attributed to photochemical and biological processing and differences in molecular weight (see for example Osburn et al., 2011). Higher spectral slopes have been attributed to autochthonous material of recent production (Zhang et al., 2011). Spectral slope data decreased from dry season to wet season, which works in tandem with the other data conclusions, as spectral slope data is inversely proportional to fluorescence data. For dry season, spectral slopes S1, S2, and S3 had average values of 0.017 nm^{-1}, 0.018 nm^{-1}, and 0.017 nm^{-1} respectively (S1 standard deviation of 0.0012 nm^{-1} ; S2 0.0028 nm^{-1} ; and S3 0.0014 nm^{-1} respectively). For wet season, spectral slopes S1, S2, and S3 had average values of 0.015 nm^{-1}, 0.012 nm^{-1}, and 0.015 nm^{-1} respectively (S1 standard deviation of 0.00079 nm^{-1} ; S2 0.00088 nm^{-1} ; and S3 0.00053 nm^{-1} respectively). On the contrary, spectral slope ratio data showed an increased between dry and wet season, positively correlating with fluorescence data. S_R had an average value of 1.01 ± 0.15 for dry season, and a value of 1.22 ± 0.076 for wet season, which was a statistically significant change between seasons (P-value 0.0014 from student t-test).

Date	A	C	T	A/C	T/C	FIX	HIX	BIX
14th July 2020	2658.57	971.37	-	2.74	-	1.24	2.38	0.72
20th July 2020	2834.63	1118.63	2091.95	2.53	1.87	1.28	1.92	0.74
28th July 2020	2804.26	1179.18	-	2.38	-	1.29	6.38	0.68
4th Aug 2020	2852.08	1277.81	-	2.23	-	1.27	4.27	0.68
11th Aug 2020	3132.79	1305.22	980.15	2.40	980.15	1.26	2.31	0.70
18th Aug 2020	3534.41	1636.45	-	2.16	-	1.36	3.26	0.66
1st Sept 2020	3174.38	1528.73	-	2.08	-	1.33	4.14	0.73
8th Sept 2020	3967.22	2013.04	-	1.97	-	1.35	3.04	0.75
24th Sept 2020	21475.62	9707.40	-	2.21	-	1.26	4.03	0.57
29th Sept 2020	5745.15	2396.79	-	2.40	-	1.30	3.87	0.64
8th Oct 2020	4285.69	1703.54	-	2.52	-	1.33	3.75	0.67
13th Oct 2020	7259.22	2942.62	-	2.47	-	1.23	5.23	0.63
27th Oct 2020	4591.12	2336.46	-	1.96	-	1.30	4.87	0.63
3rd Nov 2020	6030.90	2530.28	-	2.38	-	1.29	5.00	0.59
10th Nov 2020	7225.73	3056.36	-	2.36	-	1.25	4.82	0.55
24th Nov 2020	5802.48	2454.06	-	2.36	-	1.28	5.58	0.58
Average	5460.89	2384.87	1536.05	2.32	491.01	1.29	4.05	0.66

Table 1: Study-Wide Fluorescence Data. Intensity values of peak A, C, and T are measured in counts per second.

Date	Abs350	S1	S2	S3	SR
14th July 2020	0.0678	0.0159	0.0242	0.0164	0.6758
20th July 2020	0.0665	0.0165	0.0163	0.0168	1.0290
28th July 2020	0.0682	0.0159	0.0160	0.0164	1.0229
4th Aug 2020	0.0784	0.0161	0.0154	0.0182	1.1811
11th Aug 2020	0.0668	0.0168	0.0171	0.0175	1.0221
18th Aug 2020	0.0774	0.0167	0.0166	0.0166	1.0028
1st Sept 2020	0.0713	0.0168	0.0165	0.0164	0.9913
8th Sept 2020	0.0605	0.0195	0.0180	0.0203	1.1235
24th Sept 2020	0.1093	0.0138	0.0111	0.0145	1.3117
29th Sept 2020	0.2208	0.0134	0.0121	0.0139	1.1495
8th Oct 2020	0.1375	0.0144	0.0136	0.0147	1.0803
13th Oct 2020	0.2920	0.0146	0.0114	0.0145	1.2726
27th Oct 2020	0.1339	0.0158	0.0133	0.0158	1.1889
3rd Nov 2020	0.2243	0.0153	0.0120	0.0150	1.2449
10th Nov 2020	0.2745	0.0152	0.0117	0.0148	1.2657
24th Nov 2020	0.2049	0.0147	0.0118	0.0147	1.2445
Average:	0.1346	0.0157	0.0148	0.0160	1.1129

Table 2: Study-Wide Absorbance Data. Absorbance values measured at 350 nm. All spectral slope values are measured in nm^{-1}.

Peak1 of "Signal"	Peak1 of "Signal"
X	Y
365.5	0
366	-1.72226
366.5	-4.29556

Table 3: Raman Peak Area Data. Raman Peak Area Calibration data calculated from Origin 2016 on October 20th, 2020.

4. Conclusions

Based on optical properties, both wet and dry season at Hoag's Pond is dominated by allochthonous terrestrial sources of CDOM. Additionally, data suggests that there is proportionally more CDOM in wet season as compared to dry season. Differences in conductivity, TDS, and salinity are statistically significant between seasons, while difference in pH is not. Finally, peak A and C intensities, as well as HIX and BIX values and spectral slope ratio data, are all statistically different between seasons.

5. Acknowledgements

I would like to thank Bailey Klinger for advising me on CDOM protocol as well as Emma Nordlund for teaching me the calculations for analysis. Finally, I would like to thank Dr. Catherine Clark for her direction, guidance, and knowledge during the entire study process.

6. References

Bellingham, WA Weather History | Weather Underground [Internet]. [cited 2020 Nov 30]. Available from: https://www.wunderground.com/history/monthly/us/wa/bellingham/KBLI/date/2020-11.

Bittar T.B., Stubbins A., Vieira A.A. H., Mopper K. 2015. Characterization and photodegradation of dissolved organic matter (DOM) from a tropical lake and its dominant primary producer, the cyanobacteria *Microcystis aeruginosa*. Mar. Chem. 177, 205-217.

Boyle, E. S.; Guerriero, N.; Thiallet, A.; Vecchio, R. D.; Blough, N. V. 2009. Optical Properties of Humic Substances and CDOM: Relation to Structure. Environ. Sci. Technol., 43 (7), 2262–2268. https://doi.org/10.1021/es803264g.

Clark, C.D., L. P. Litz, and S.B. Grant. 2008. Saltmarshes as a source of chromophoric dissolved organic matter to Southern California coastal waters. Limnol. Oceanogr. 53, 1923-1933.

Clark, C.D., Aiona, P., Keller, J.K., De Bruyn, W.J., 2014. Optical characterization and distribution of chromophoric dissolved organic matter (CDOM) in soil porewater from a salt marsh ecosystem. Mar. Ecol. Prog. Ser. 516, 71-83.

Coble, P.G. 1996. Characterization of marine and terrestrial DOM in seawater using excitation emission matrix spectroscopy. Mar. Chem. 51, 325-346.

De Laurentiis E., Minella M., Maurino V., Minero C., Brigante M., Mailhot G., Vione D. 2012. Photochemical production of organic matter triplet states in water samples from mountain lakes, located below or above the tree line. Chemosphere 88, 12108-1213.

Green, S. A.; Blough, N. V. 1994. Optical Absorption and Fluorescence Properties of Chromophoric Dissolved Organic Matter in Natural Waters. Limnology and Oceanography, 39 (8), 1903–1916. https://doi.org/10.4319/lo.1994.39.8.1903.

Hansen AM, Kraus TEC, Pellerin BA, Fleck JA, Downing BD, Bergamaschi BA. Optical properties of dissolved organic matter (DOM): Effects of biological and photolytic degradation. Limnol. Oceanogr. 2016 May;61:1015–1032.

Hu, C., Muller-Karger, F.E., Zepp, R.G., 2002. Absorbance, a(300) and apparent quantum yield: a comment on common ambiguity in the use of these optical concepts. Limnol. Oceanogr, **47**: 1261-1267.

Hu B., Wang P., Qian J., Wang C., Zhang N., Cui X. 2017. Characteristics, sources and photobleaching of chromophoric dissolved organic matter (CDOM) in large and shallow Hongze Lake, China. J. Great Lakes Res. 43, 1165-1172.

Huguet, A., Vacher, L., Relexans, S., Saubusse, S., Froidefone, J.M., Parlanti, E., 2009. Properties of fluorescent dissolved organic matter in the Gironde Estuary. Organic Geochemistry. 40: 706-719.

Kieber, R. J.; Whitehead, R. F.; Reid, S. N.; Willey, J. D.; Seaton, P. J. 2005. Chromophoric Dissolved Organic Matter (CDOM) In Rainwater, Southeastern North Carolina, USA. J Atmos Chem, 54 (1), 21–41. https://doi.org/10.1007/s10874-005-9008-4.

Kutser T., Pierson D.C., Kallio K.Y., Reinart A., Sobek S. 2005. Mapping lake CDOM byv remote sensing. Remote Sesing of Environ. 94, 535-540.

Laurion I., Ventura M., Catalan J., Psenner R., Sommaruga. 2000. Attenuation of ultraviolet radiation in mountain lakes: factors controlling the among- and within-lake variability. Limnol. Ocean. 45, doi: 10.4319/lo.2000.45.6.1274.

McKnight, D.M. and G.R. Aiken, 1998. Sources and age of aquatic humus, p.9-40. *In* D.O. Hessen and L.J. Tranvik [eds.], Ecological studies: Aquatic humic substances. Springer-Verlag.

McKnight, D.M., Boyer, E.W., Westerhoff, P.K., Doran, P.T., Kulbe, T., Andersen, D.T., 2001. Spectrofluorometric characterization of dissolved organic matter for indication of precursor organic material and aromaticity. Limnol. Oceanogr. 46: 38-48.

Moran, M.A. and R.G. Zepp, 1997. Role of photoreactions in the formation of biologically labile compounds from dissolved organic matter. Limnol. Oceanogr. 42: 1307-1316.

Mostofa K.M., Yoshioka T., Konohira E., Tanoue E. 2007. Dynamics and characteristics of fluorescent bdissolved organic matter in the groundwater, river and lake water. Water, Air and Soil Poll, 184, 157-176.

Nebbioso, A.; Piccolo, A. 2013. Molecular Characterization of Dissolved Organic Matter (DOM): A Critical Review. Anal Bioanal Chem, 405 (1), 109–124. https://doi.org/10.1007/s00216-012-6363-2.

Obernosterer I. and Benner R. 2004. Competition between biological and photochemical processes in the mineralization of dissolved organic carbon. Limnol. Ocean. 49, doi: 10.4319/lo.2004.49.1.0117.

Ohno, T. 2002. Fluorescence Inner-Filtering Correction for Determining the Humification Index of Dissolved Organic Matter. Environ. Sci. Technol., 36 (4), 742–746. https://doi.org/10.1021/es0155276

Osburn, C. L.; Wigdahl, C. R.; Fritz, S. C.; Saros, J. E. 2011. Dissolved Organic Matter Composition and Photoreactivity in Prairie Lakes of the U.S. Great Plains. Limnol. Oceanogr., 56 (6), 2371–2390. https://doi.org/10.4319/lo.2011.56.6.2371.

Qui Y., Shi H., Jing H., Cai Q., Takemura M., Haraguchi S. 2012. Characterization and variations of dissolved organic matter in the Lake Taihu area of China. Water Supply 12, 439-450.

Song K., Li S., Wen Z., Lyu L., Shang Y. 2019. Characterization of chromophoric dissolved organic matter in lakes across the Tibet-Qinghai Plateau using spectroscopic analysis. J. Hydrol. 579, 124-190.

Song K., Shang Y., Wen Z., Jacinthe P-A., Liu G., Lyu L., Fang C. 2019. Characterization of CDOM in saline and freshwater lakes across China using spectroscopic analysis. Water Res. 150, 403-417.

Stedmon, C.A., Markager, S., Bro, S., 2003. Tracing disolved organic matter in aquatic environments using a new approach to fluorescence spectroscopy. Mar. Chem. **82**: 219-254.

Stedmon, C.A., Markager. S., 2005. Resolving the varaibility in dissolved organic matter fluorescence in a temperate estuary and its catchment using PARAFAC analysis. Limnol. Oceaongr. 50, 686 – 697.

Tranvik, L.J., Downing, J.A., Cotner, J.B., Loiselle, S.A., Striegl, R.G., Ballatore, T.J., Dillon, P., Finlay, K., Fortino, K., Knoll, L. B., Kortelainen, P. L., Kutser, T., Larsen, S., Laurion, I., Leech, D. M., Mccallister, S. L., Mcknight, D. M., Melack, J. M., Overholt, E., Porter, J. A., Prairie, Y., Renwick, W. H., Roland, F., Sherman, B.S., Schindler, D.W., Sobek, S., Tremblay, A., Vanni, M.J., Verschoor, A.M., Wachenfeldt, E.Von, and Weyhenmeyer, G. A. 2009. Lakes and reservoirs as regulators of carbon cycling and climate, Limnol. Oceanogr., 54, 2298–2314.

Urban N.R., Auer M.T., Green S.A., Lu X., Apul D.S., Powell K.D., Bub L. 2005. Carbon cyclin in Lake Superior. J. Geophys. Res. 110, doi: 10.1029/2003JC00230

Vione, D.; Minella, M.; Maurino, V.; Minero, C. 2014. Indirect Photochemistry in Sunlit Surface Waters: Photoinduced Production of Reactive Transient Species. Chem. Eur. J., 20 (34), 10590–10606. https://doi.org/10.1002/chem.201400413.

Zhang Y., van Djik M.A., Liu M., Zhu G., Quin B. 2009. The contribution of phytoplankton degradation to chromophoric dissolved organic matter (CDOM) in eutrophic shallow lakes: field and experimental evidence. Water Res. 43, 4685-4697.

Zhang Y., Yin Y., Liu X., Shi S., Feng L., Liu M., Zhu G., Gong Z., Quin B. 2011. Spatial-seasonal dynamics of chromophoric dissolved organic matter in Lake Taihu, a large eutrophic shallow lake in China. Org. Geochem. 42, 510-519.

Zhao Y., Song K., Wen Z., Fang C., Shang Y. Lv L. 2017. Evaluation of CDOM sources and their links with water quality in the lakes of Northeast China using fluorescence spectroscopy J. Hydrolog. 550, 80-91.

Zhou Z., Guo L., Minor E.C. 2016. Characterization of bulk and chromophoric dissolved organic matter in the Laurentian Great Lakes during summer 2013. J. Great Lakes Res. 42, 789-801.

Zsolnay, A., Baigar, E., Jimenez, M., Steinweg, B., Saccomandi, F., 1999. Differentiating with fluorescence spectroscopy the sources of dissolved organic matter in soils subjected to drying. Chemosphere. 38: 45-50.